Electronic Supplementary Material (ESI) for Chemical Science.

Supporting Information

An efficient factor for fast screening of high-performance two-dimensional metal-organic frameworks towards catalyzing oxygen evolution reaction

Computational details: The initial model structures are all based on the previously reported 2D MOFs (Cambridge Crystal Data Center, No. 638866) except for the metal ions were replaced by twenty kinds of different transition metal elements. In this work, all the spin-polarized density-functional theory (DFT) computations in this work were performed via the Cambridge Sequential Total Energy Package (CASTEP)[1-2] with the pseudopotential plane wave (PPW) method.[3] The interaction between electrons and ions was described using the ultrasoft pseudopotentials (USP) that proposed by Vanderbilt.[4] A plane-wave basis set was employed to expand the smooth part of the wave functions with a kinetic cutoff energy of 600 eV. For the electron-electron exchange and correlation interactions, the functional parametrized by Perdew-Burke-Ernzerhof for solid (PBESOL)[5], a form of the general gradient approximation (GGA), was used throughout to obtain the accurate structural configuration. Due to the correlation effect is insufficient considered by standard DFT, the DFT+U method is adopted in this work. All the U values used in this work are obtained from calculation based on the linear response method proposed by Damian A. Scherlis [6] rather than the empirical U parameters.

The desired surface was modelled with a monolayers of MOFs since the MOFs studied in this work is a kind of natural 2D MOFs. To eliminate the interaction between the periodic images, a suffciently large vacuum region of 15Å was added along the *c* axis of the unit cell. Considering the adsorbates on only one side of the slab model, the self-consistent dipole correction was applied to achieve higher accuracy.[7] The solvent effect was described via the explicit solvent model according to the previous report.[8]

During the geometry optimizations process, all the atom positions were allowed to relax. The Brillouin-zone integrations were conducted using Monkhorst-Pack (MP) grids of special points.[9] A (5 × 3 × 1) *k*-point grid was used for the surface cell. The water and hydrogen molecules were calculated in a (20 × 19 × 18) $Å^3$ box to avoid the possible degeneracy and the Brillouin-zone integrations were performed using the Gamma-point-only grid. The convergence criterion for the electronic self-consistent field (SCF) loop was set to 10^{-6} eV/atom. The atomic structures were optimized until the residual forces were below 0.03 $eVÅ^{-1}$, and the cell parameters were also optimized

with finite basis correction for bulk cell until the stress were less than 0.05 GPa.

Synthesis of 2D MOFs: The 2D MOFS was prepared via a solvothermal method. First of all 1.0 mmol of terephthalic acid (PTA), 0.1 mmol of sodium hydroxide (NaOH) and 1.5 mmol of corresponding chloride, namely, $NiCl_2 \cdot 6H_2O$ for Ni-MOFs, $CoCl_2 \cdot 6H_2O$ for Co-MOFs, $FeCl_2$ for Fe-MOFs, $ZnCl_2$ for Zn-MOFs and VCl_2 for V-MOFs, were dissolved in 20 mL *N*,*N*-dimethylformamide (DMF) in a 50 mL beaker. After stirring at room temperature for 1 h, the solution was transferred to a 50 mL reaction kettle and keep the temperature at 120 °C for 12 h. After cooling to room temperature, the product was washed with ethanol three times. Then, the precipitates were dried via freeze drying in vacuum.

Characterizations: The field emission-scanning electron microscope (SEM) images were recorded by a Zeiss SUPAR 55 field emission-scanning electron microscope (FE-SEM). The transmission electron microscopy (TEM) images were obtained through a field emission high resolution transmission electron microscopy (FE-TEM) (JEOL JEM-2010). The X-ray diffraction (XRD) spectra were measured on a Bruke D8 Advance diffractometer (Cu Kα1). The AFM measurements were recorded by a SPM-960 microscope. The XPS was carried out on a Thermo escalab 250 Xi X-ray photoelectron spectrometer. The nitrogen adsorption-desorption isotherm was performed at 77 K by an ASAP 2020 system.

Electrochemical measurements: The electrochemical measurements were conducted using a Princeton PMC 1000 & 500 electrochemical workstation. All the measurements were carried out in 1M KOH solution with the three-electrode configuration, and all potentials measured were calibrated to the reversible hydrogen electrode (RHE) through the following equation: E_{RHE} = Emeasured + 0.24 V + 0.0592 pH. To prepare the work electrode for the subsequent measurements, the catalysts ink (ethanol was used as solution) were uniformly dropped on the gold rotating disk electrode (RDE) to employed as the working electrode (a mass loading of 0.4 mg cm^{-2}, the rotate speed

was set to 1200 rpm unless other stated). Saturate calomel electrode (SCE) was used as the reference electrode (RE), and platinum slice (1 cm × 1 cm) was chosen as the counter electrode (CE). To obtain an accurate result, the scan rate for linear sweep voltammetry (LSV) was set to 5 mV s^{-1} to minimize the capacitive current.

(a)

Sc 5.94	Ti 8.11	V 7.52	Cr 6.98	Mn 7.27	Fe 7.85	Co 7.42	Ni 8.86	Cu 7.43	Zn 7.78
Y 7.53	Zr 5.21	Nb 7.79	Mo 8.74	Tc 7.82	Ru 5.54	Rh 6.73	Pd 7.55	Ag 6.92	Cd 8.85

(b)

Sc -0.63	Ti -0.66	V -0.78	Cr -0.75	Mn -0.59	Fe -0.61	Co -0.64	Ni -0.61	Cu -0.59	Zn -0.72
Y -0.72	Zr -0.61	Nb -0.57	Mo -0.66	Tc -0.69	Ru -0.67	Rh -0.76	Pd -0.68	Ag -0.71	Cd -0.73

(c)

Sc 5.87	Ti 8.01	V 7.49	Cr 6.84	Mn 7.21	Fe 7.79	Co 7.40	Ni 8.78	Cu 7.38	Zn 7.72
Y 7.49	Zr 5.18	Nb 7.72	Mo 8.66	Tc 7.76	Ru 5.50	Rh 6.69	Pd 7.47	Ag 6.88	Cd 8.77

(d)

Sc -0.57	Ti -0.62	V -0.71	Cr -0.67	Mn -0.51	Fe -0.58	Co -0.61	Ni -0.60	Cu -0.52	Zn -0.69
Y -0.66	Zr -0.58	Nb -0.54	Mo -0.62	Tc -0.65	Ru -0.61	Rh -0.70	Pd -0.63	Ag -0.65	Cd -0.71

Figure. S1. (a) The zero point energy (ZPE) of different metal-based M-OO (unit: kcal/mol). (b) The value of contribution from entropy to the Gibbs free energy (*TS* term) of different metal-based M-OO (unit: eV). (c) The zero point energy (ZPE) of different metal-based M-O (unit: kcal/mol). (d) The value of contribution from entropy to the Gibbs free energy (*TS* term) of different metal-based M-O (unit: eV).

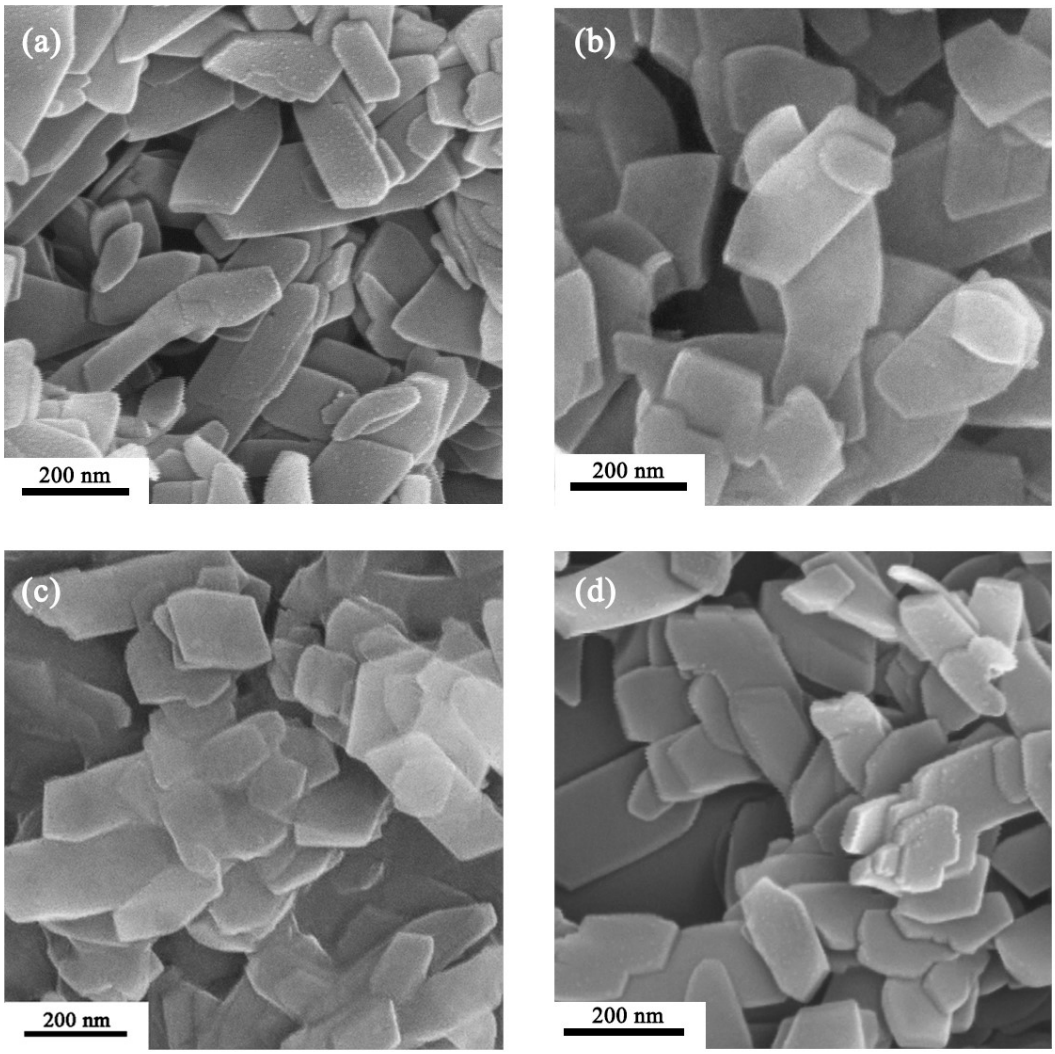

Figure S2. SEM images of different MOFs-nanosheets：(a) Ni-MOFs, (b) Co-MOFs, (c) Fe-MOFs and (d) Mn-MOFs.

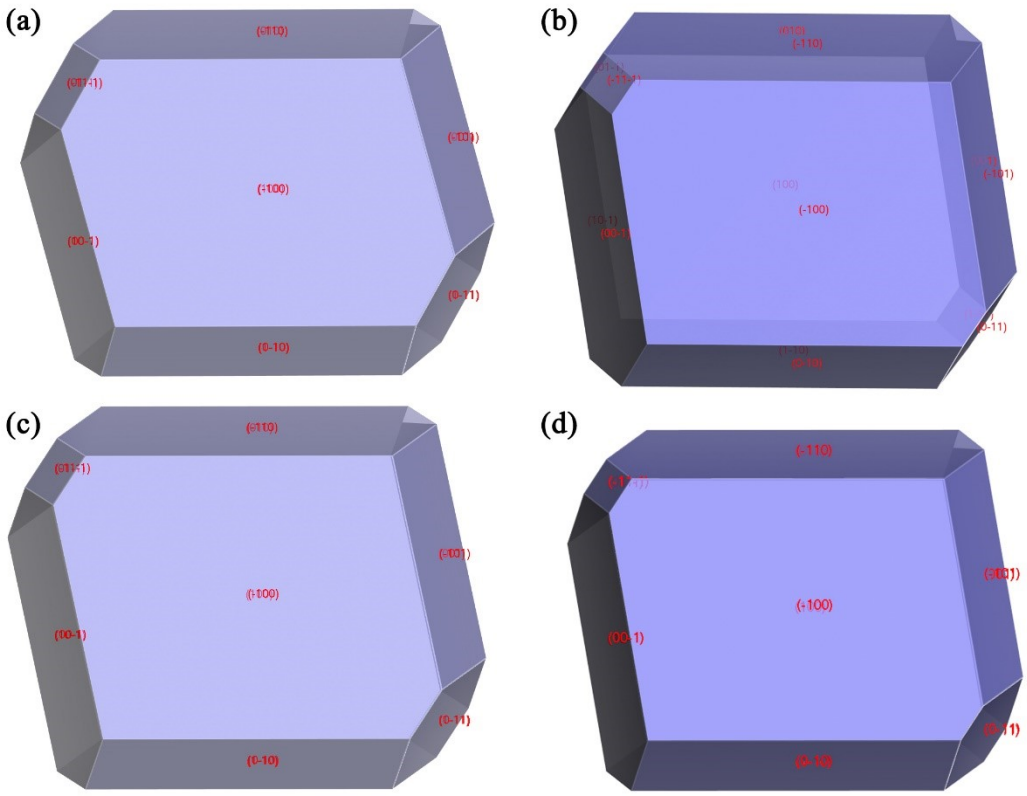

Figure S3. Tridimensional BFDH morphology of different metal-based 2D MOFs. As shown in figures above, the MOFs nanosheets possess an obvious 2D flake-like structure and the largest exposed plane is (-100).

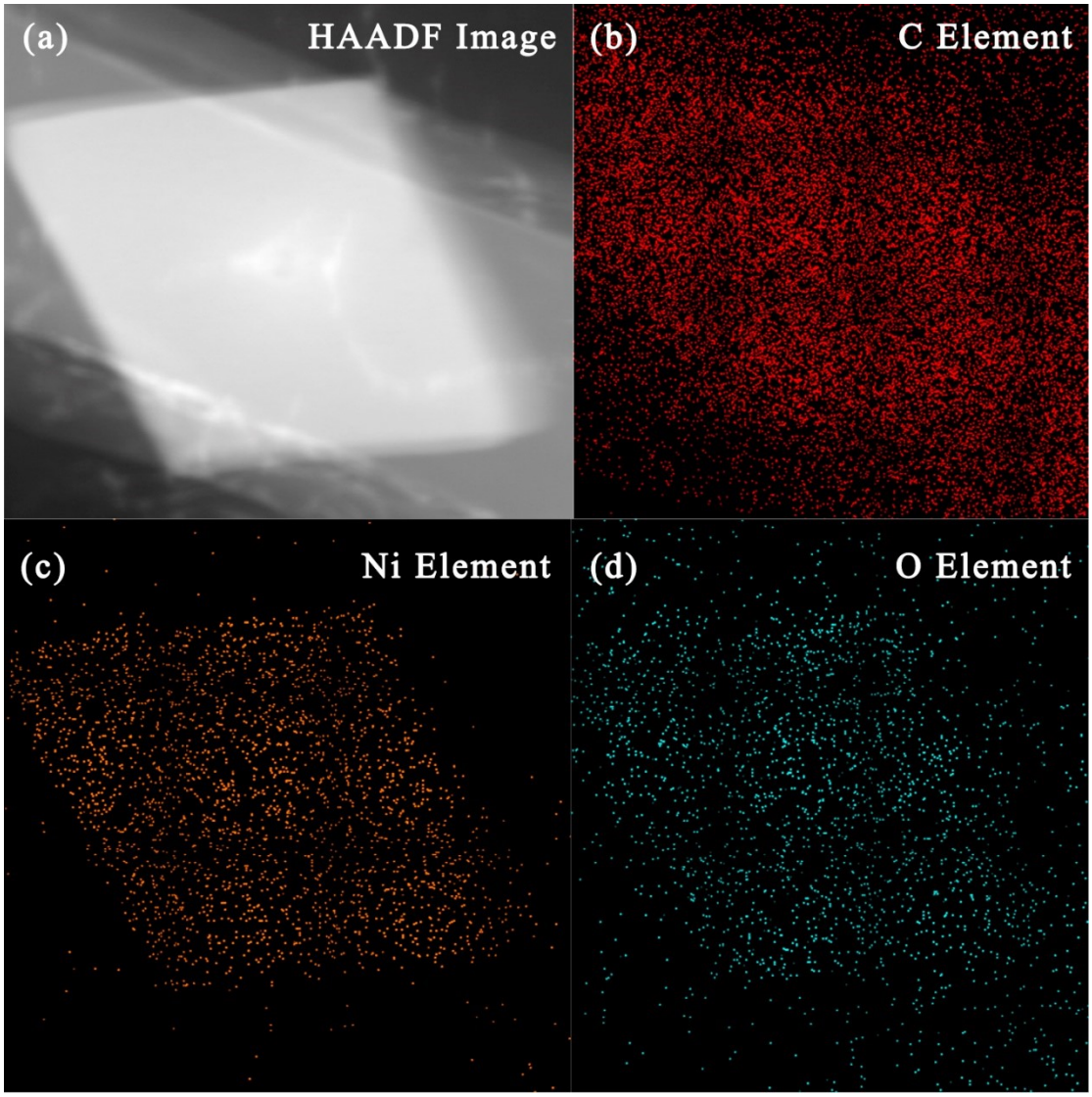

Figure S4. (a) HAADF image of Ni-MOFs, (b) EDS mapping image of C element, (c) EDS mapping image of Ni element, (d) EDS mapping image of O element.

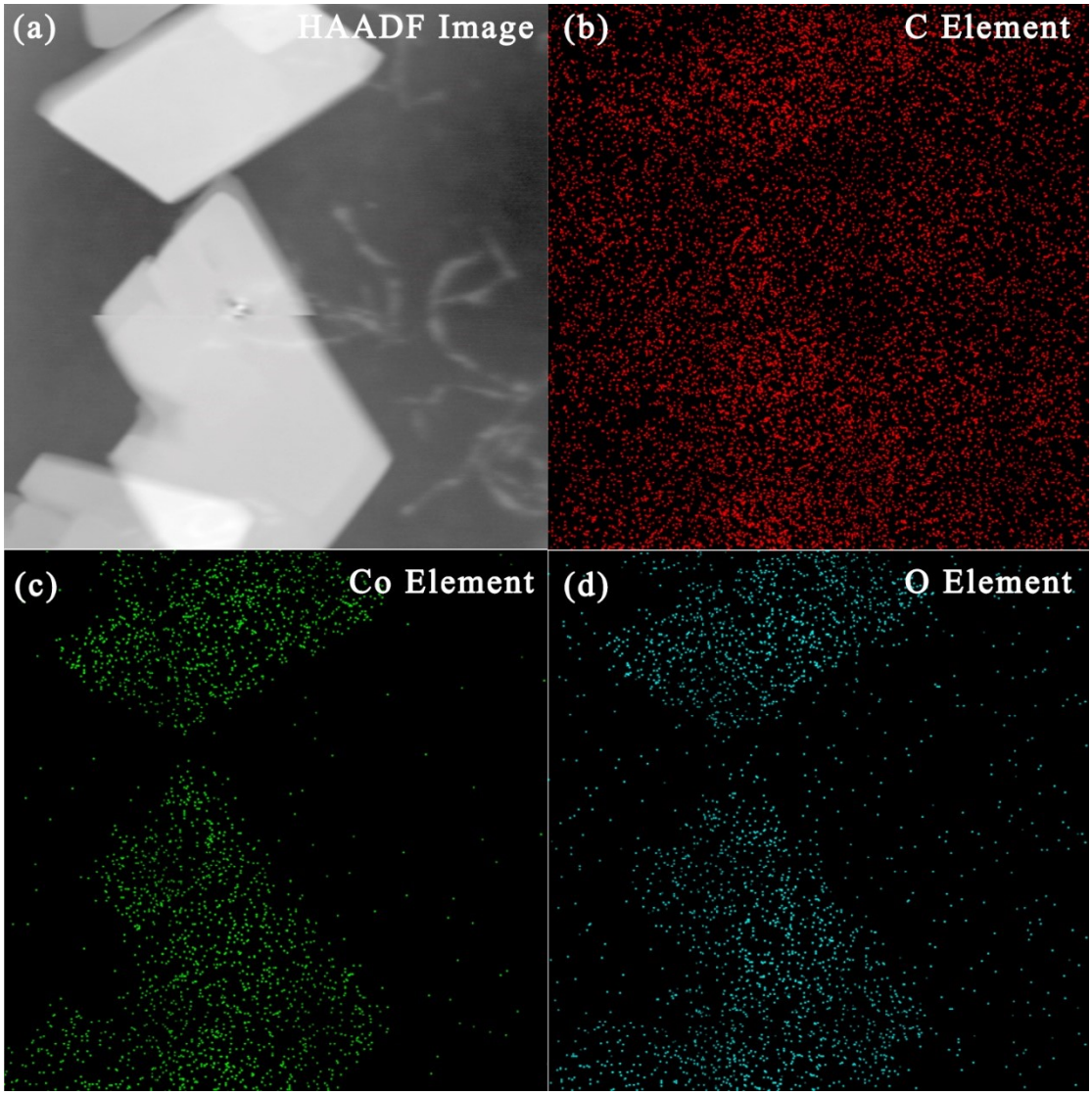

Figure S5. (a) HAADF image of Co-MOFs, (b) EDS mapping image of C element, (c) EDS mapping image of Co element, (d) EDS mapping image of O element.

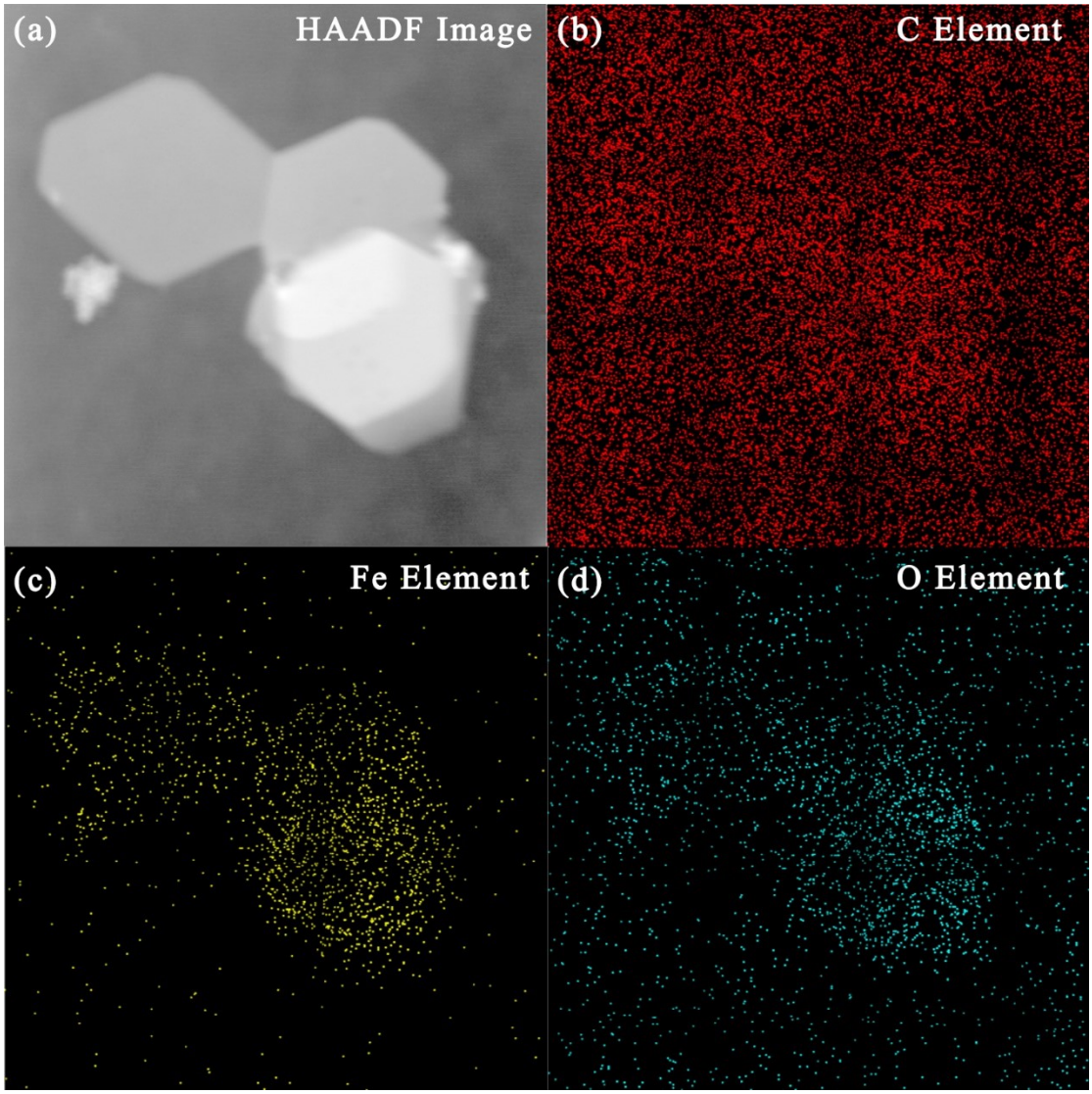

Figure S6. (a) HAADF image of Co-MOFs, (b) EDS mapping image of C element, (c) EDS mapping image of Fe element, (d) EDS mapping image of O element.

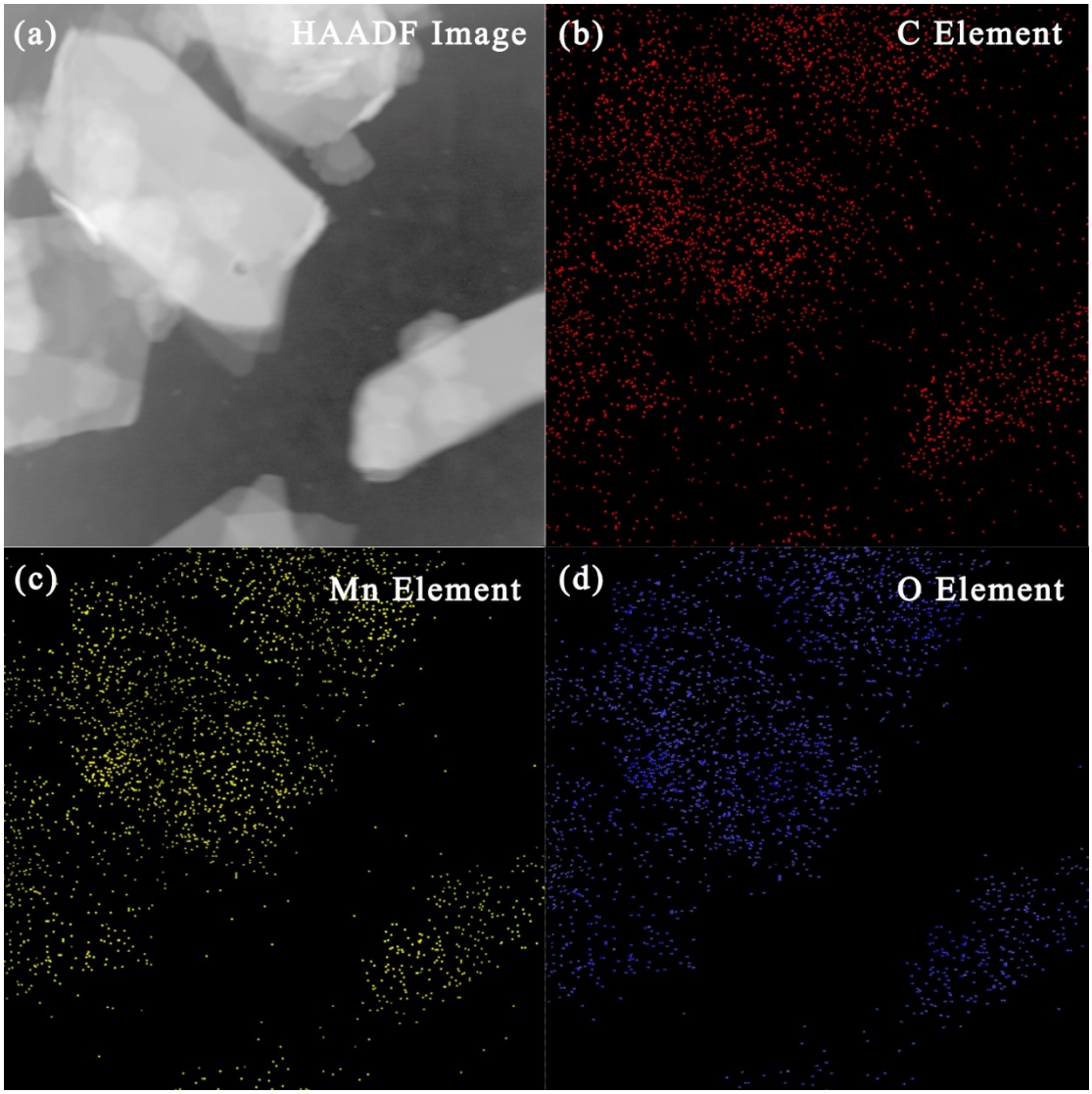

Figure S7. (a) HAADF image of Co-MOFs, (b) EDS mapping image of C element, (c) EDS mapping image of Mn element, (d) EDS mapping image of O element.

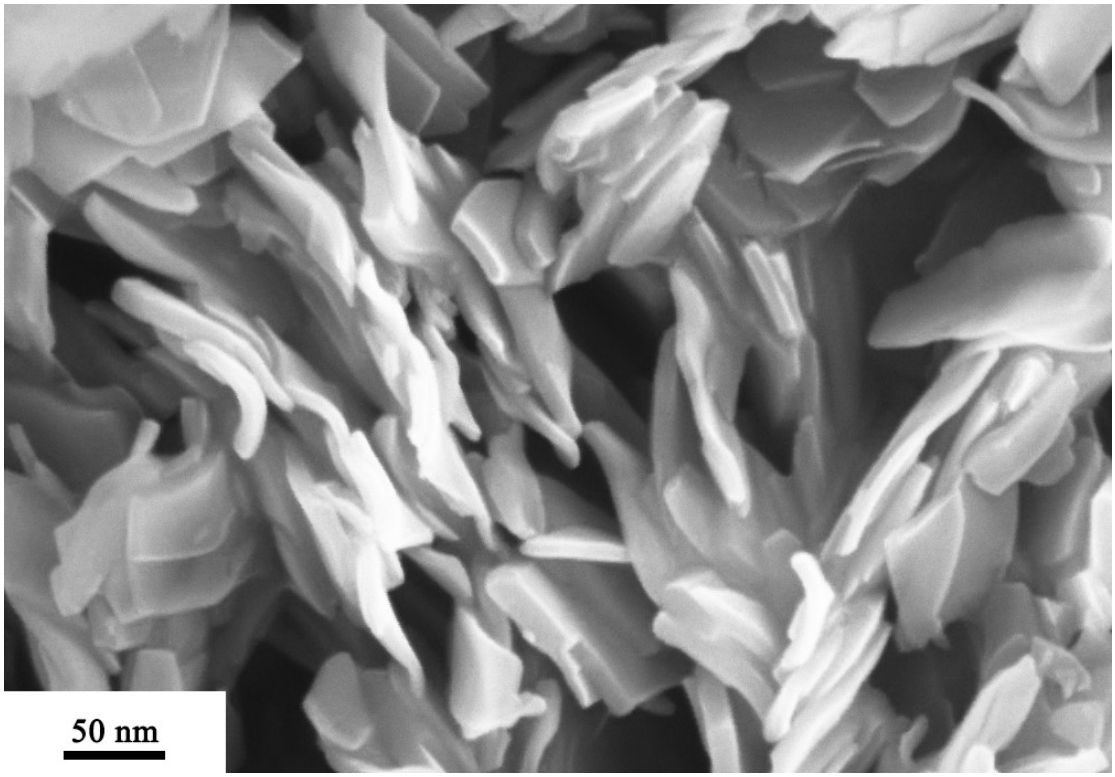

Figure S8. Side view of the 2D Ni-MOFs, indicating the thickness of the single layer is about 10 nm.

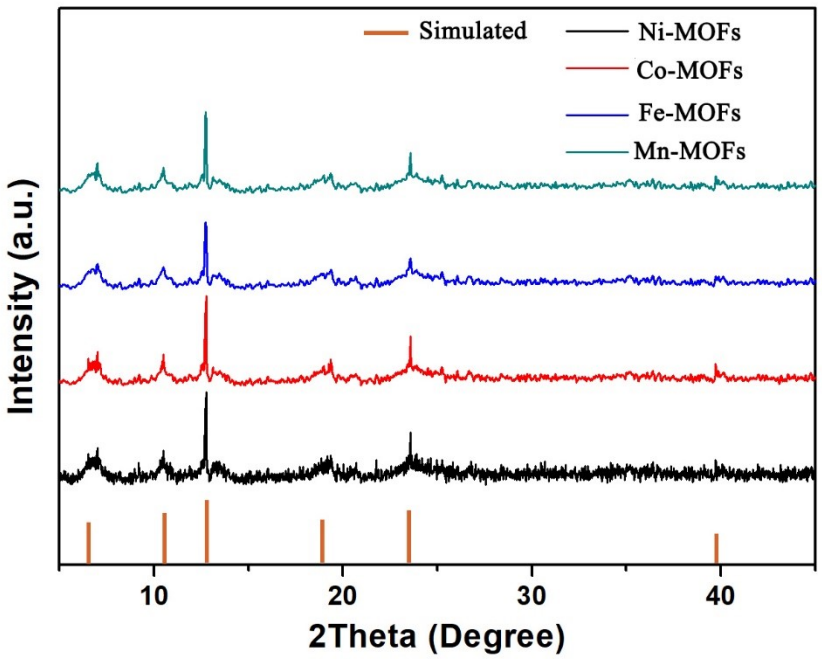

Figure S9. The experimentally observed PXRD patterns of Ni-MOFs, Co-MOFs, Fe-MOFs, Mn-MOFs and the simulated pattern of the optimized Ni-MOFs. This results indicate the as-prepared MOFs are isostructural to the previously reported 2D-MOFs. Note that the double peak at about 6º should be assigned to the Kα1 and Kα2, which could also be observed at other peaks but not obvious.

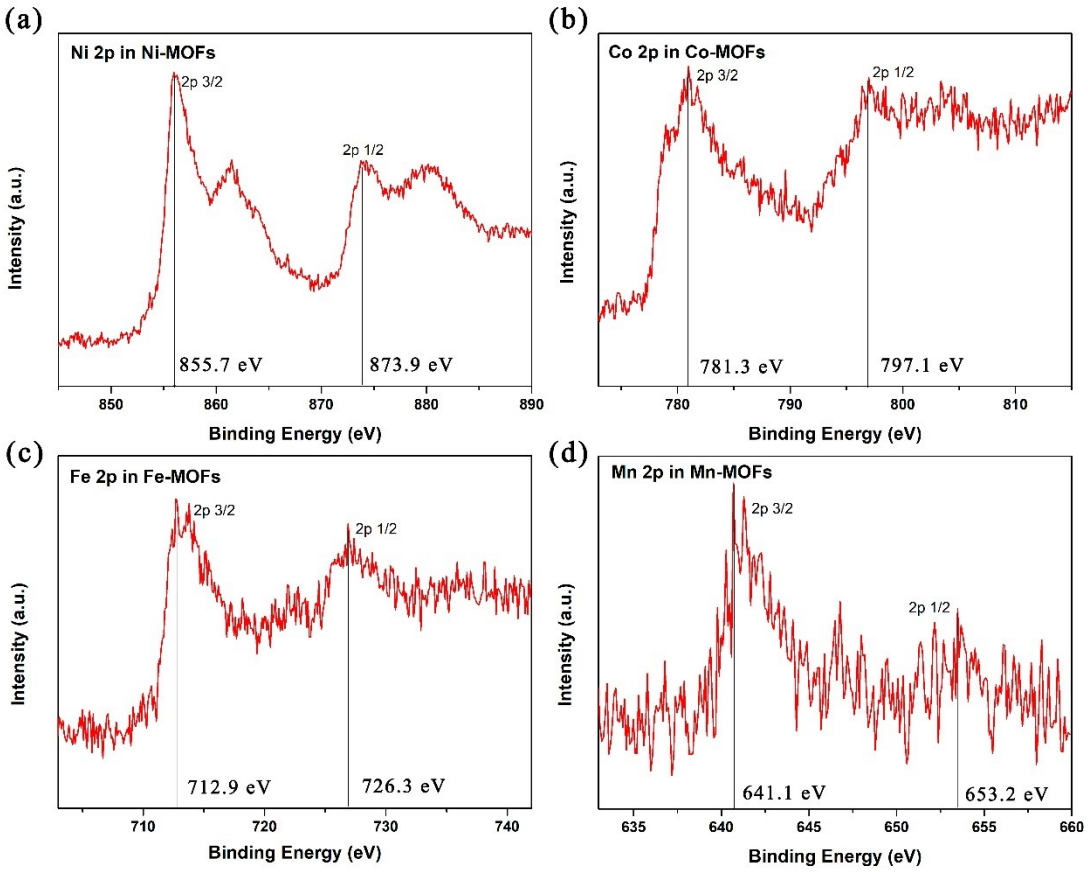

Figure S10. High-resolution XPS spectrum of (a) Ni 2p in Ni-MOFs, (b) Co 2p in Co-MOFs, (c) Fe 2p in Fe-MOFs and (d) Mn 2p in Mn-MOFs.

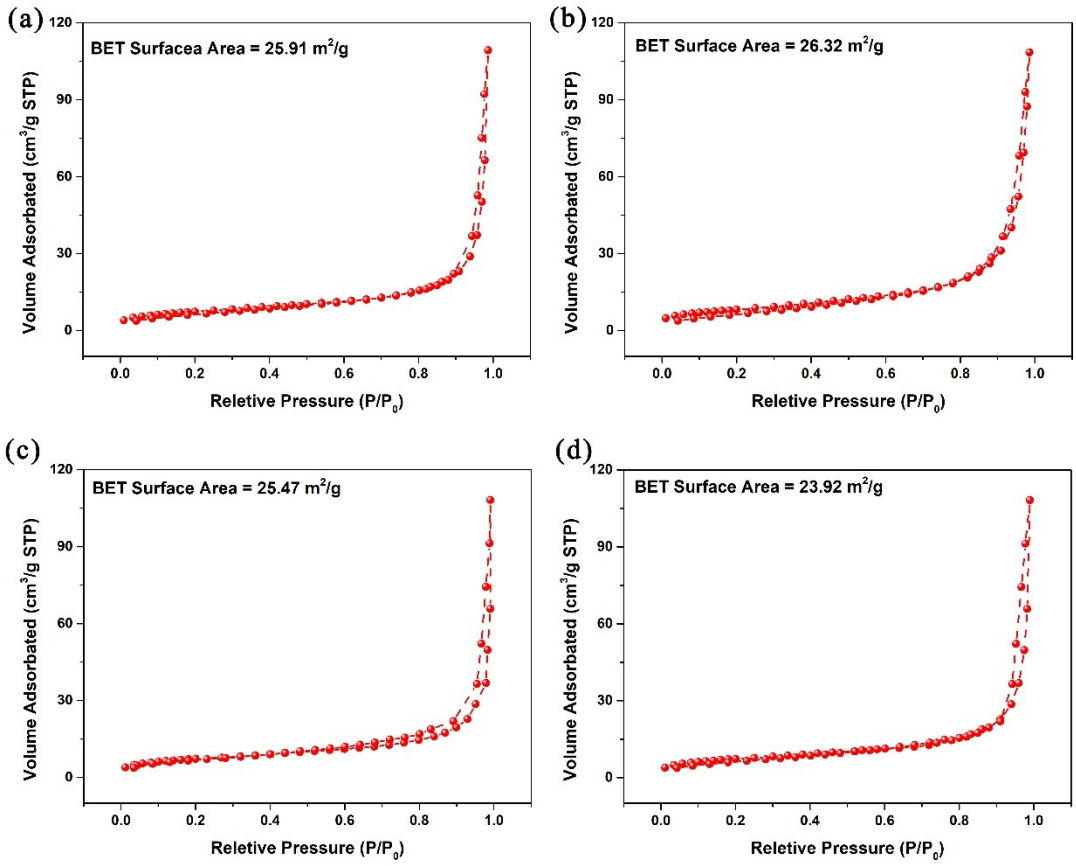

Figure S11. N_2 adsorption-desorption isotherm at 77 K of (a) Ni-MOFs, (b) Co-MOFs, (c) Fe-MOFs and (d) Mn-MOFs.

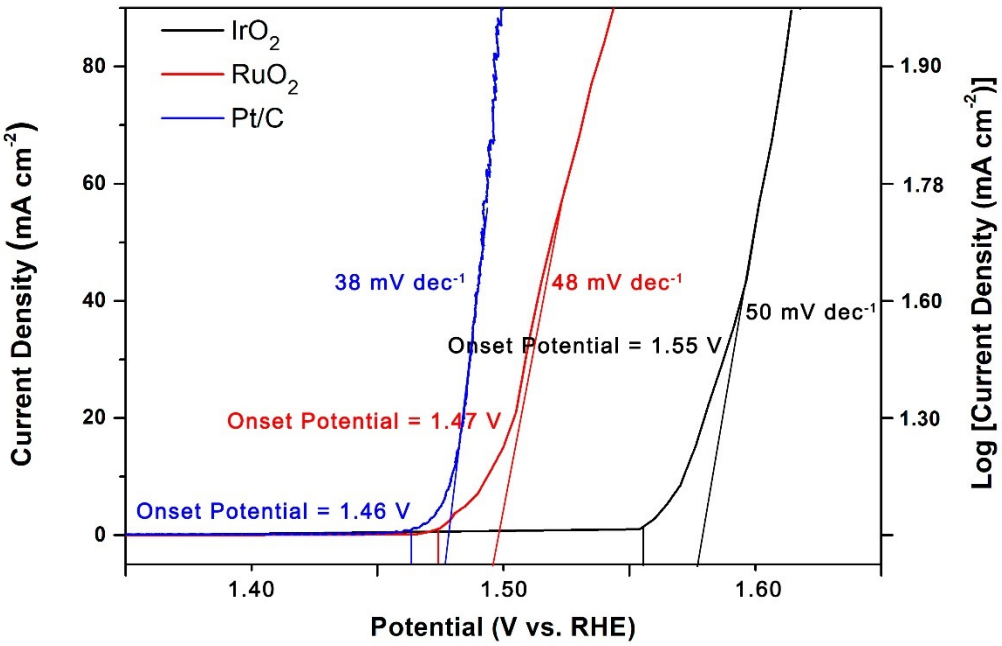

Figure S12. LSV curves of RuO_2, IrO_2 and Pt/C.

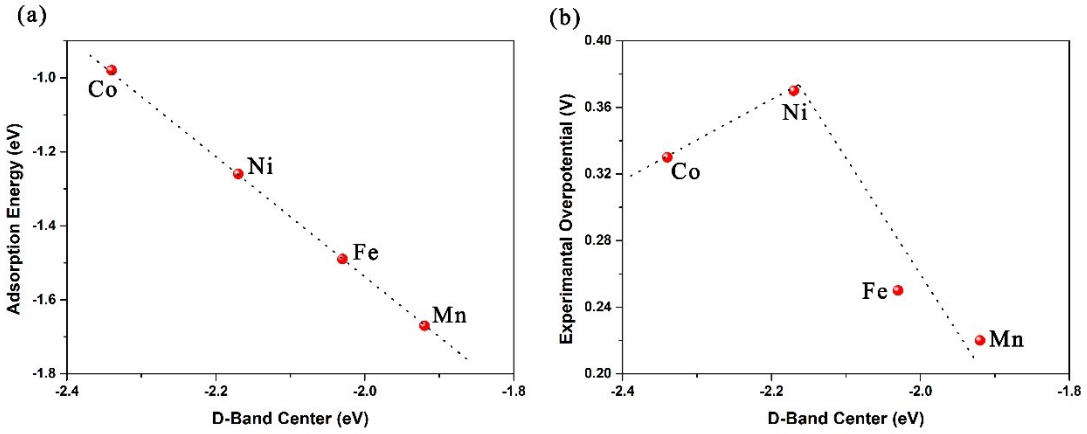

Figure S13. Correlation between d-band center and (a) adsorption energy of *OH and (b) experimental overpotential.

Reference

[1] Clark S J, Segall M D, Pickard C J, et al. First principles methods using CASTEP. Zeitschrift für Kristallographie-Crystalline Materials, 2005, 220(5-6): 567-570.

[2] Segall M D, Lindan P J D, Probert M J, et al. First-principles simulation: ideas, illustrations and the CASTEP code. Journal of Physics: Condensed Matter, 2002, 14(11): 2717.

[3] Troullier N, Martins J L. Efficient pseudopotentials for plane-wave calculations. Physical Review B, 1991, 43(3): 1993.

[4] Laasonen K, Car R, Lee C, et al. Implementation of ultrasoft pseudopotentials in ab initio molecular dynamics. Physical Review B, 1991, 43(8): 6796.

[5] Perdew J P, Ruzsinszky A, Csonka G I, et al. Restoring the density-gradient expansion for exchange in solids and surfaces. Physical Review Letters, 2008, 100(13): 136406.

[6] Kulik H J, Cococcioni M, Scherlis D A, et al. Density functional theory in transition-metal chemistry: A self-consistent hubbard U approach. Physical Review Letters, 2006, 97: 103001.

[7] Neugebauer J, Scheffler M. Adsorbate-substrate and adsorbate-adsorbate interactions of Na and K adlayers on Al (111). Physical Review B, 1992, 46(24): 16067.

[8] Zhao X, Liu Y. Unveiling the active structure of single nickel atom catalysis: critical roles of charge capacity and hydrogen bonding. Journal of American Chemical Society, 2020, 142(12): 5773–5777.

[9] Monkhorst H J, Pack J D. Special points for Brillouin-zone integrations. Physical Review B, 1976, 13(12): 5188.